JOURNAL OF GEOPHYSICAL RESEARCH, VOL. 92, NO. B7, PAGES 6215–6221, JUNE 10, 1987

Omori's Power Law Aftershock Sequences of Microfracturing in Rock Fracture Experiment

TAKAYUKI HIRATA

Department of Geophysics, Faculty of Science, Kyoto University, Kyoto, Japan

A time series of acoustic emissions (AE) in basalt was measured under constant uniaxial compression. Some bursts of AE events considered to be the main shock and aftershock sequences were observed. Two models describing the aftershock sequences (the exponential decay model, $n(t) = K \exp(-pt)$, and the Omori's power law model, $n(t) = K/(c + t)^p$, where $n(t)$ denotes the occurrence rate of aftershocks at time t) were examined. With the progress of the fracturing process, the bursts changed from the exponential decay type to Omori's power law type, and the p value of Omori's power law aftershock sequences decreased. These results indicate that microfracturing gains a longer tail with the evolution of the fracture process. The reproduction of Omori's power law aftershock sequences of AE events suggests that the self-similarity of rock fracturing holds good over a range from microfracturing to large earthquakes.

INTRODUCTION

The series of statistical studies on the occurrence of shallow earthquakes by *Kagan and Knopoff* [1978, 1980*a*, *b*, 1981] showed that the seismic process has a stochastic self-similarity in time and space dimensions, which holds good over a magnitude range from $M = 1.5$ to the greatest earthquake. This self-similarity manifests itself in the power law: For example, in size distribution it corresponds to Gutenberg-Richter's magnitude-frequency relation; in spatial distribution it is the relation of $N(r) \sim r^D$, where $N(r)$ is the number of events within the distance r from a given event; in time series it is Omori's power law for the rate of occurrence of aftershocks and foreshocks. A question arises as to whether we can extend this self-similarity down to the scale of microfracturing.

Since aftershock sequences are observed universally on the earth, *Scholz* [1968*a*] assumed that if microfracturing is truly similar to seismicity, some sort of aftershock sequence should be reproducible in the laboratory. He succeeded in reproducing Omori's power law aftershock sequences of acoustic emission (AE) events by isolating the rock specimen intactly from the axial stress just after the whole fracture of the rock sample. In his experimental reproduction he considered that the fracture of the whole rock specimen corresponded to the main shock and AE corresponded to the aftershocks. However, the question "Is this correspondence right?" still remains; the fracture of the whole rock specimen may correspond to the fracture of the whole tectonic plate, and AE events may correspond to the earthquakes (from main shocks to aftershocks). If the self-similarity in rock fracturing truly holds good down to the scale of microfracturing, we can find Omori's power law aftershock sequences even in microfracturing activity. Scholz's study does not provide sufficient evidence to show that Omori's power law is an intrinsic nature in the rock fracturing process and that the self-similar structure holds good from microfracturing (10^{-6} m) to large earthquakes (10^5 m).

To determine whether Omori's power law aftershock sequences are intrinsic phenomena in rock fracturing, a constant stress rock fracture experiment was carried out. The time series of AE events were measured during the experiment, and the main shock and aftershock sequences were sought in a time series of AE events. The bursts of AE events that were considered as the main shock and aftershock sequences were analyzed to examine whether or not aftershock sequences of AE events obey Omori's power law. The exponential decay model is considered to be an alternative model for the aftershock sequences of AE events. *Akaike* [1974] showed that we can select the best fit model between several competing models on the measurement using Akaike's information criterion (AIC). We compared the exponential decay model and Omori's power law model by AIC based on a time series of AE events.

Paper number 7B1003.
0148-0227/87/007B-1003$05.00

EXPERIMENTAL TECHNIQUE

The rock studied is commercially known as Murata basalt. The specimen was a right circular cylinder, 110.0 mm in height and 44.5 mm in diameter with ends ground parallel to within ± 0.005 mm. The rock specimen was vacuum-dried for 24 hours and stored in a desiccator for 2 months. To prevent water intrusion from the atmosphere during the experiment, the specimen was coated with a 0.5-mm-thick layer of silicon.

Figure 1 shows the schematic diagram of the loading apparatus, the strain monitoring system, and the AE time series measurement system. A servo-controlled hydraulic testing machine was used for loading. Axial and circumferential strains of the cylindrical specimens were measured by cross-type electrical resistance gauges 20 mm in length. Three gauges were mounted at 120° intervals in the center section of the specimen. A piezoelectric lead zironate titanate (PZT) transducer with a resonant frequency of 1 MHz was mounted on the center of the specimen to detect the AE events and was covered by a copper cap to reduce electromagnetic noise.

To obtain a time series of AE events with the magnitude, both the origin time and the magnitude of each AE event were measured simultaneously. A signal from the PZT transducer was fed into the magnitude discriminator after being amplified by 40 dB (effective frequency range 10 kHz to 1 MHz). The magnitude discriminator classified the AE event into eight steps set equally on a logarithmic scale (threshold levels were set 10, 21.5, 46.5, 100, 215, 465, 1000, and 2150 mV) when the magnitude discriminator judged the signal as an AE event. A microcomputer read both the magnitude and the origin time of each AE event with the magnitude discriminator and the

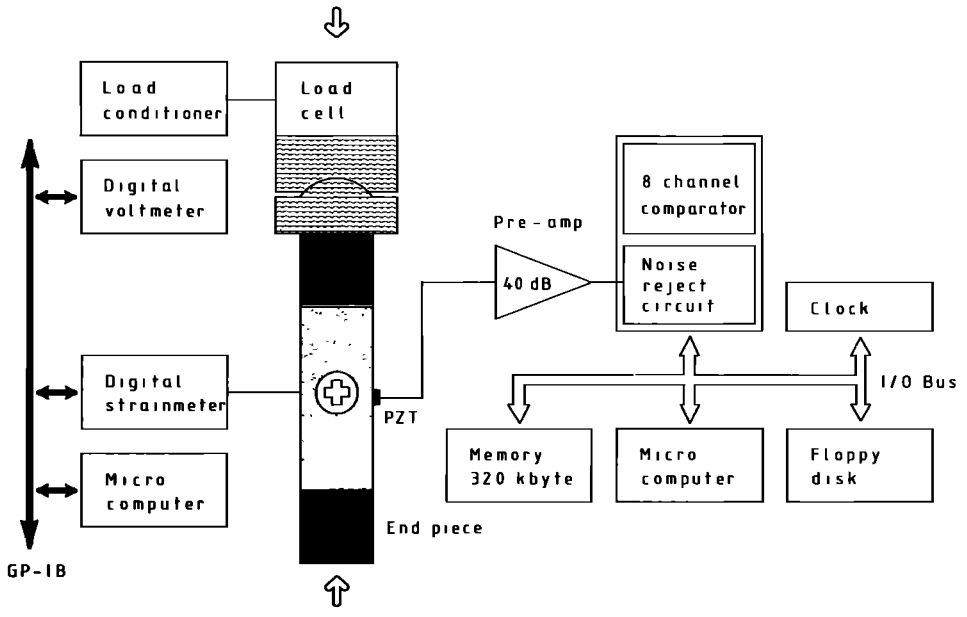

Fig. 1. Block diagram of the experimental system for strain and AE time series measurement. A PZT transducer and three cross-type strain gauges were mounted on the rock sample.

external clock, respectively. The data were stored in RAM memory via an I/O bus. The number of the maximum measurable AE events per second was about 800, and the maximum number of storable AE without a break was about 80,000. The resolution of the detection time was 1 ms. When the RAM memory became full, the microcomputer stopped data acquisition and transferred the data from RAM memory to a floppy disk. The details of the time series measurement system was described by *Hirata et al.* [1984].

EXPERIMENTAL RESULTS

Strain and AE Rate

A constant stress of 275 MPa was applied. This was about 85% of the fracture strength of Murata basalt that was obtained in the constant stress rate loading experiments (1×10^{-2} MPa/s). Fluctuation of the axial stress during the creep was controlled to less than $\pm 0.05\%$. Figure 2 shows the strains against axial stress for Murata basalt. The volumetric strain was calculated from the circumferential strain and axial strain, in which each strain was obtained by the average of three strain gauges. Figure 3 shows the strains against time for Murata basalt. The volumetric strain produced a creep curve that had three stages; at the primary stage the strain rate decreased transiently, at the secondary stage the strain rate was almost constant, and at the tertiary stage the strain rate accelerated. Figure 4 shows the AE rate against time during the experiment, where AE rate is the number of AE events per 10 s. AE rate increased during loading, decreased exponentially after loading, increased gradually, and increased super exponentially just prior to the fracture. Unfortunately, the data acquisition system was blind during 8970–10,260 s when the data was being transferred from the RAM memory to the floppy disk.

Bursts of AE events were observed during the creep. Each burst was regarded as a mainshock and aftershock sequence. The series of large bursts were numbered as bursts 1–7, as shown in Figure 4. Figure 5 shows the plot of the time series of each burst. The first event with a magnitude larger than 7 in each burst was regarded as the main shock, which is marked by S in Figure 5. When the occurrence rate of AE events approached an almost constant rate (that near the rate at the time before the occurrence of the main shock), we marked it, T, the end of the aftershock sequences in Figure 5.

Model Selection With AIC

Two models describing the time series characteristics of aftershock sequences were considered. One is Omori's power law model, which is written as

$$n(t) = K/(C + t)^p \tag{1}$$

and the other is the exponential decay model expressed by

$$n(t) = K \exp(-pt) \tag{2}$$

Here K, C, p are constants, and $n(t)\,dt$ denotes the frequency of aftershocks occurring between time t and $t + dt$ (t is measured from the origin time of the main shock).

Ogata [1983] proposed the maximum likelihood method to estimate the parameters of the modified Omori's formula for aftershock sequences directly based on a time series of aftershocks. Ogata's method is reviewed briefly in the following lines. The occurrence of aftershock sequences is treated by a nonstationary Poisson point process. By using the intensity function $n(t)$, a nonstationary Poisson point process is completely characterized [*Liptser and Shiryayev*, 1978]. An intensity function is defined by

$$n(t) = \lim_{\Delta t \to 0} \text{Prob}\{\text{an event in } [t, t + \Delta t)\}/\Delta t \tag{3}$$

The likelihood function with the intensity function is ex-

pressed as

$$f(t_1, t_2, \cdots, t_N; N) = \left\{\prod_i n(t_i)\right\} \exp\left\{-\int_a^T n(t)\, dt\right\} \quad (4)$$

where $\{t_i;\ i = 1, 2, \cdots, N\}$ are the occurrence times of the events on a time interval [S, T] which is the period of observation. Time was measured from time S, that is, the time of the occurrence of the main shock. The parameters that maximize the likelihood function (4) were calculated, and the statistical model identification is carried out according to AIC.

Akaike [1974] introduced the information theoretic criterion (AIC) estimate (MAICE) for the statistical model selection. When several competing models are involved, the AIC is defined by

$$\text{AIC} = (-2)\ \max\ (\text{log likelihood}) + 2(\text{number of independently adjusted parameters within the model}) \quad (5)$$

A model with a smaller AIC is considered as a better fit. If the difference of the values of AIC between two models is larger than 1, we can select the model with a smaller AIC as the fit model that fits the data significantly better. The parameters were estimated, and the models were selected for seven bursts according to the procedure proposed by *Ogata* [1983]. As the intensity function on nonstationary Poisson point process, we used two functions: Omori's power law expressed in equation (1) and the exponential decay model in equation (2).

The parameters that maximize the log likelihood function of the model was estimated for the data of time interval [S, T] that is shown in Figure 5, by using the algorithm of the searching maximum value [*Davidon*, 1968]. The effect of the AE events that occurred independently of the main shock was eliminated because the number of AE events that depend on the main shock was much larger than that of the independent AE events in the bursts. To consider the effect of the time interval [S, T] on the estimated parameters, we carried out the estimation of the parameters in a different time interval [S, T*]. The estimated parameters were almost independent of the time interval, and almost the same result was obtained.

Table 1 shows the calculated values of the parameters and AIC for the bursts. AIC is calculated from equation (5). According to the AIC, the better fit model for burst 1, 2 is the exponential decay model, and that for burst 3, 4, 5, 6, 7 is Omori's power law model. Figure 6 shows the frequency of the bursts against time on double logarithmic coordinates. In Figure 6, the open circles indicate the actual data, the solid curve indicates Omori's power law model with the parameters estimated by a maximum likelihood procedure (listed in Table 1), and the dashed curve indicates the exponential model with the parameters estimated by the maximum likelihood procedure (listed in Table 1). Note that we obtained the model lines from the original time sequence data, not from the frequency data shown by the open circles in Figure 6. To see the stability of the p value in the models, we added homogeneous random events to the actual data by 3% and calculated the parameter for the resulting time sequences. This was done 10 times for each sequence, and Table 2 shows the fluctuation of the p value for the models due to the additional random events. The fluctuation of the p value was about within ± 0.1, indicating that the change in the p value of Omori's power law

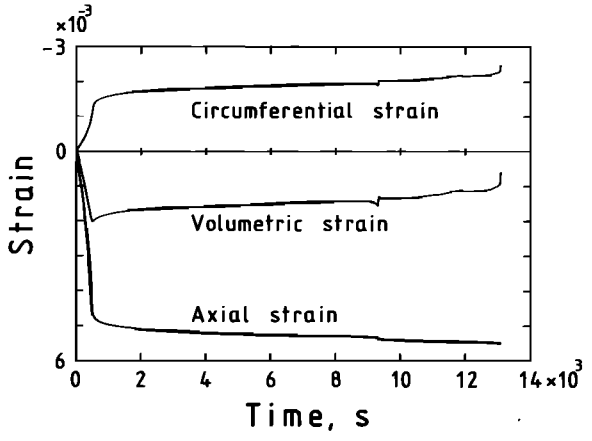

Fig. 3. Average strains against time for Murata basalt during loading and the uniaxial constant stress condition.

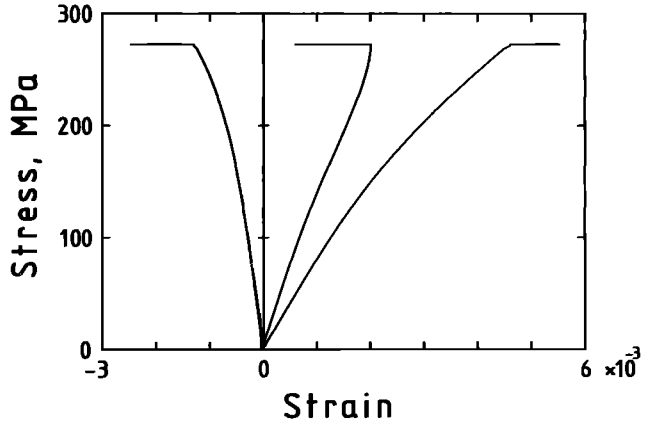

Fig. 2. Average strains against axial stress for Murata basalt. The creep stress was 275 MPa.

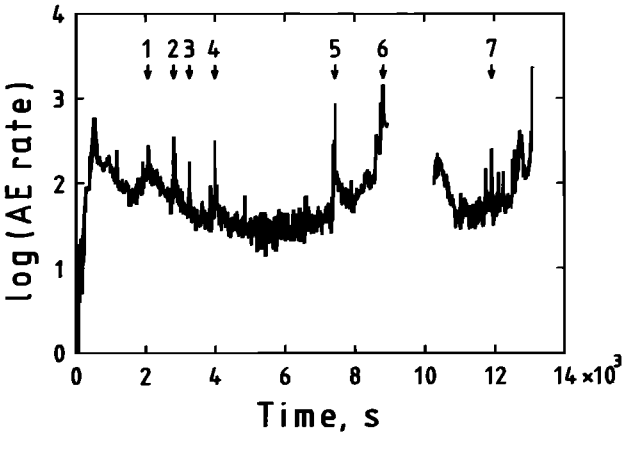

Fig. 4. The change in AE rates during loading and uniaxial constant stress condition. AE events could not be measured during the time interval of 8970–10,260 s due to transfer of the data from the RAM memory to the floppy disk. The bursts were numbered from bursts 1 to 7 as the mainshock and aftershock sequences.

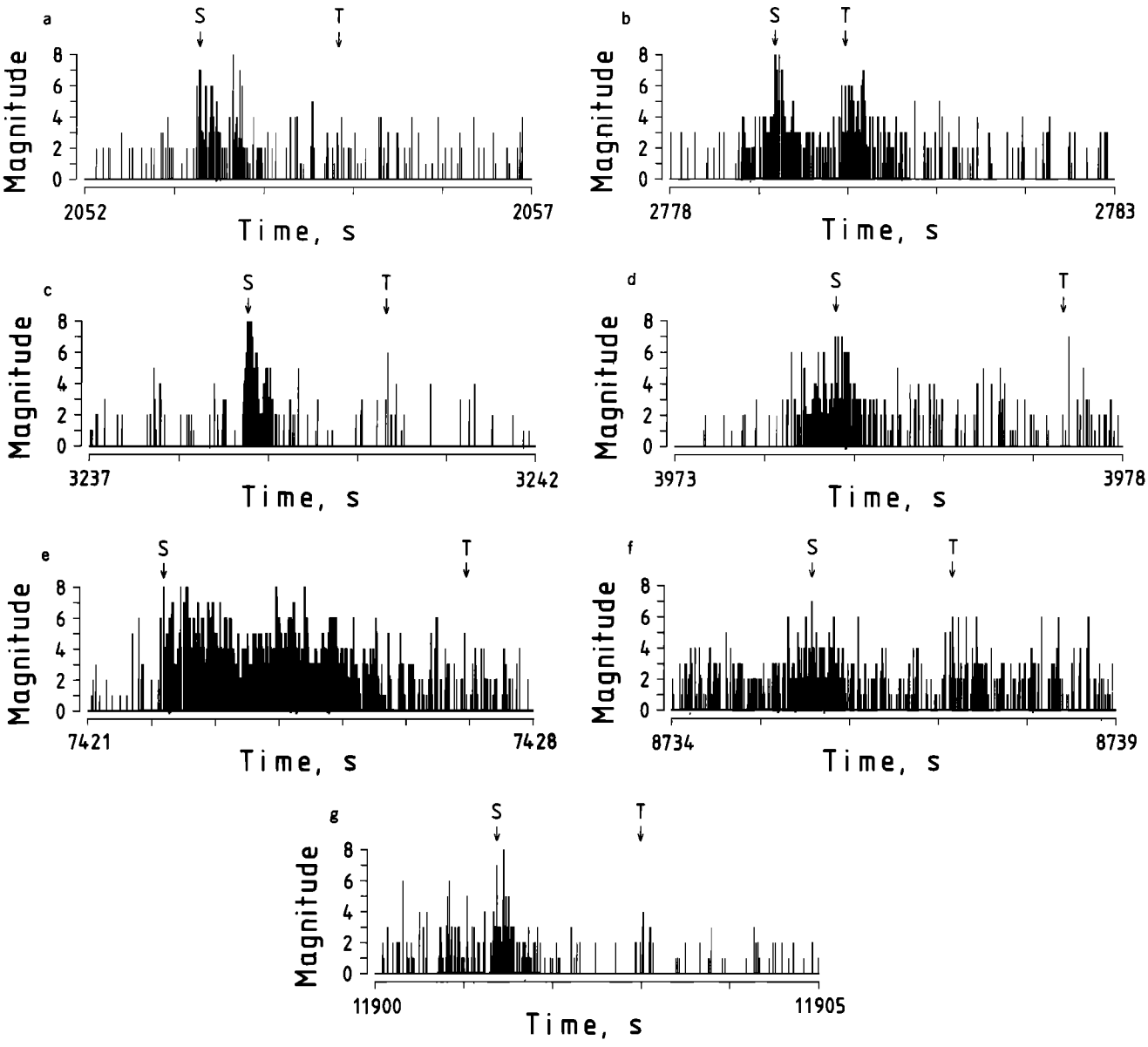

Fig. 5. Time series plots of the bursts. Main shocks are marked S, and the end of analysis interval T. The magnitude of events was determined by maximum amplitude, where AE events of magnitudes 1, 2, 3, 4, 5, 6, 7, and 8 have a maximum amplitude of 10, 21.5, 45.6, 100, 215, 456, 1000, and 2150 mV or larger after being amplified by the preamplifier at the gain of 40 dB, respectively. Bursts 1–7 correspond to Figures 5*a*–5*g*.

TABLE 1. Estimated Values of AIC and the Parameters

Burst	Model*	AIC	K	C	p
1	I	739.69	658.35	748.72	1.281
	II	737.27	0.1243	···	9.792×10^{-4}
2	I	1217.5	0.9024	41.99	0.3076
	II	1216.4	0.1932	···	5.775×10^{-4}
3	I	432.03	100000	264.75	2.270
	II	440.61	0.1851	···	3.053×10^{-3}
4	I	813.39	1499.8	826.77	1.409
	II	814.49	0.0893	···	7.416×10^{-4}
5	I	3493.0	1266.2	683.62	1.246
	II	3558.5	0.1888	···	3.658×10^{-4}
6	I	974.22	26.362	218.06	0.847
	II	975.73	0.1990	···	1.089×10^{-3}
7	I	558.16	33.979	106.83	1.059
	II	568.10	0.1119	···	1.516×10^{-3}

*Model I is Omori's power law model, and model II is the exponential decay model. Time unit is millisecond.

from burst 3 to 7 is significant. The scatter from the expected line of the better fit model may be caused by secondary aftershocks. For example, the existence of a peak at about 1 s after the main shock in Figure 6*e* indicates the existence of a secondary aftershock sequence.

DISCUSSION

Self-similarity manifests itself in the power law. For example, in size distribution, it is Gutenberg-Richter's magnitude-frequency relation. In spatial distribution it is $N(r) \sim r^D$, where $N(r)$ is the number of events within the distance r from an event. In time series it corresponds to Omori's power law for the occurrence rate of foreshocks and aftershocks. In size distribution and spatial distribution the self-similarity in rock fracturing can be extended to a scale of microfracturing. The Gutenberg-Richter relation also holds well for the scale of microfracturing in rocks [*Mogi*, 1962; *Scholz*, 1968*b*]. The

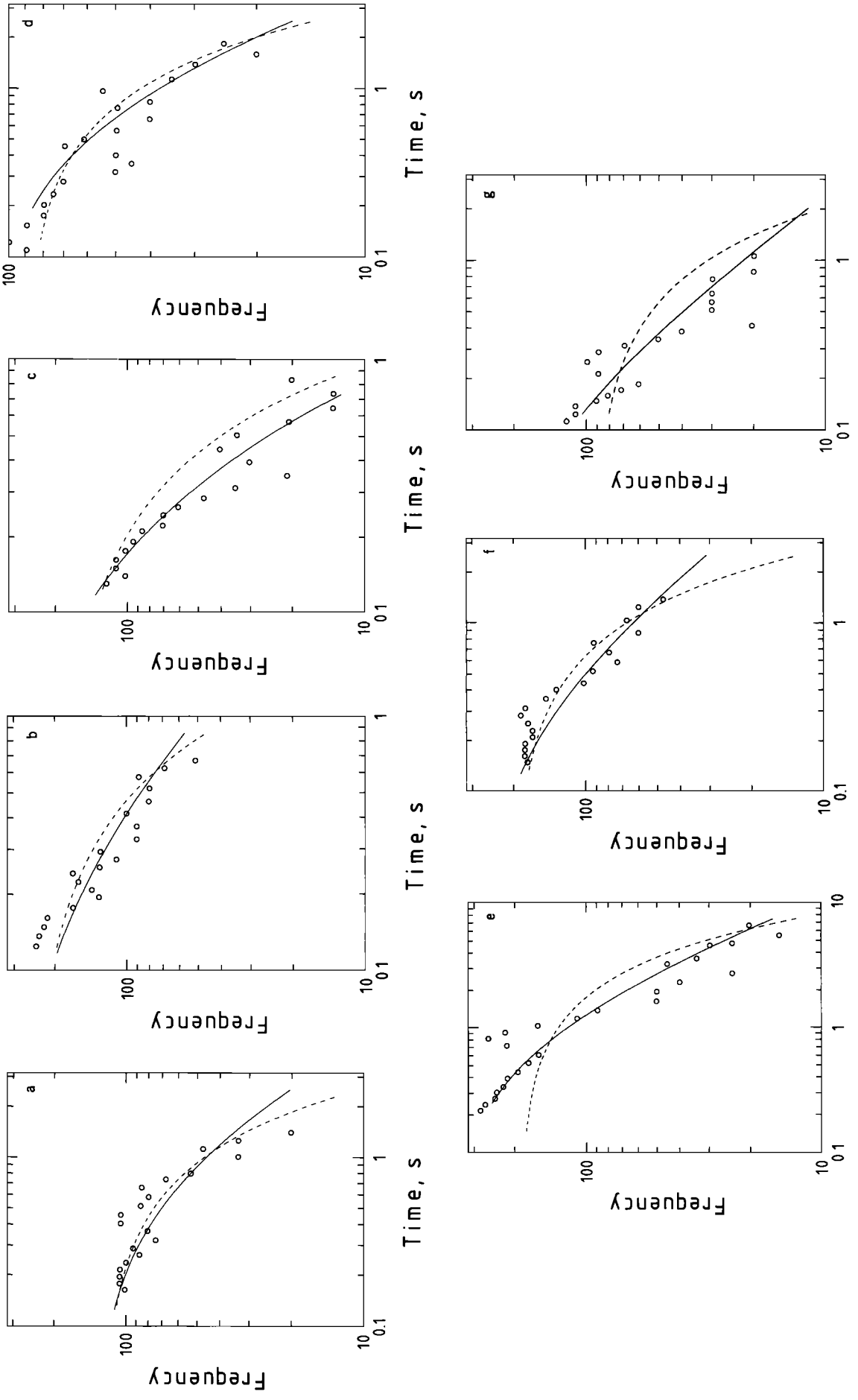

Fig. 6. Frequency of bursts against time on a logarithmic scale. Time is the time measured from the mainshock marked in Figure 5. Open circles are plots of the actual data. Solid curve is for Omori's power law decay model with the parameters listed in Table 1, and dashed curve is the exponential decay model with the parameters listed in Table 1. Bursts 1–7 correspond to Figures 6*a*–6*g*.

TABLE 2. Fluctuation of p Value

Burst	*Model I	*Model II
1	1.271 ~ 1.451	*8.610 ~ 9.792* × 10^{-4}
2	0.271 ~ 0.330	*5.405 ~ 5.991* × 10^{-4}
3	*2.270 ~ 2.255*	2.839 ~ 3.107 × 10^{-3}
4	*1.390 ~ 1.409*	6.581 ~ 7.672 × 10^{-4}
5	*1.238 ~ 1.241*	3.453 ~ 3.579 × 10^{-4}
6	*0.725 ~ 0.934*	1.008 ~ 1.084 × 10^{-3}
7	*0.959 ~ 1.068*	1.383 ~ 1.507 × 10^{-3}

*Model I is Omori's power law model, and model II is the exponential decay model. Better fit model's p value are in italics.

self-similarity in spatial distribution of the earthquake epicenter [*Kagan and Knopoff*, 1980*a*; *Sadovskiy et al.*, 1984] is also found in spatial distribution of microfracturing [*Hirata et al.*, 1987].

In time series, *Scholz* [1968*a*] showed that if the rock sample is isolated from the axial stress after the whole sample fracture, microfracturing activity decays as a function of t^{-1} in a manner similar to typical earthquake aftershock sequences. The fracture of the whole rock specimen may correspond to the fracture of the whole tectonic plate, and AE events are the earthquakes including from main shocks to aftershocks. Furthermore, the stress condition of the null stress after the occurrence of main shocks is somewhat artificial. Therefore the successful reproduction of Omori's power law aftershock sequences under a more realistic stress condition suggests that Omori's power law is intrinsic to rock fracturing. *Kagan and Knopoff* [1978, 1980*b*, 1981] showed that the rate of occurrence dependent shocks increases as t^{-1} making every earthquake a multishock event and that Omori's power law for aftershocks has been verified for catalogs of the largest earthquakes on a worldwide scale as well as for catalogs on a smaller regional scale. The results of *Kagan and Knopoff* [1978, 1980*b*, 1981] and the successful reproduction of Omori's power law aftershock sequences in the laboratory by *Scholz* [1968*a*] and this study indicate that the self-similar structure holds good from microfracturing to largest earthquakes.

The present study showed that aftershock sequences change from the exponential decay type to Omori's power law type with the progress of fracturing of the whole rock specimen. *Mogi* [1962] showed that the AE activity rate is expressed by a function of $n(t) = K \exp(-pt)$ when the stress is held constant. *Scholz* [1968*a*] found that the AE activity rate is expressed as a power law function of $n(t) = K\ t^{-1}$ after the fracture of whole rock specimen. The main difference between the reports of *Mogi* [1962] and *Scholz* [1968*a*] is the condition of the rock specimen when AE activity was measured; in Mogi's case the rock specimen was not fractured, and in Scholz's case the rock sample was fractured and AE activity was measured after the fracture. Our results may be explained by assuming that the change of the fracture condition from Mogi's to Scholz's condition occurred during the creep with the evolution of the fracture process; we can assume that the rock specimen was not fractured just after setting the creep stress (corresponds to Mogi's experimental condition), and the rock specimen approached the ultimate fracture of the rock specimen (corresponds to Scholz's experimental condition) with the progress of the creep.

The difference between Omori's power law decay and exponential decay is rather small when t, the time after the main shock, is not large but is substantial when t is large. Omori's power law aftershock sequences last longer than the exponential decay aftershock sequences because the decay rate of the power law function is slower than that of the exponential decay function. Furthermore, the p value of Omori's power law for aftershocks decreased gradually with the evolution of the fracture process. The aftershock with a smaller parameter p has a longer tail of seismic activity. This means that microfracturing has a longer tail with the evolution of the fracture process.

On the basis of the fault model that has different asperity, *Mikumo and Miyatake* [1979] showed that the value of parameter p in Omori's power law decreases with increasing the heterogeneity of the frictional strength distribution. If the heterogeneity of the rock sample increases with the evolution of the fracture process, our results support their finding.

When the considered rock fracturing as a stochastic process, the self-similarity in magnitude, space, and time dimensions held good over a scale of 10^{-6} to 10^{5} m. The geometry of the fracture surface of rocks has also a self-similar structure; *Mandelbrot* [1967] showed that a coastline that is a large scale rock surface is a fractal (fractal is a general concept of self-similarity introduced by Mandelbrot). *Brown and Scholz* [1985] showed that the topography of natural rock surfaces, such as joints and faults, is a fractal. *King* [1983] showed that the fault system that consists of mainfaults and minor subfaults is self-similar. These facts suggest that the process of rock fracturing is self-similar from microfracturing to large earthquakes. We do not claim, however, that the fracture process is strictly self-similar. Since *Scholz and Aviles* [1986] suggest that the large and small earthquakes belong to different hierarchies of size distribution, the value of the scaling parameter may change in a different scale range.

Based on the self-similar property of rock fracturing, a scale invariant fracture mechanism has been considered by some investigators [*Allégre et al.*, 1982; *Madden*, 1983; *Smalley et al.*, 1985; *Turcotte et al.*, 1985; *Turcotte*, 1986]. If the theory of the scale invariant fracture process is valid in rock fracturing, our finding can be extended directly to the seismicity of earthquakes. Our findings indicate that the decrease in the p value is useful for the prediction of large earthquakes and that the p value can be used for the estimation of the degree of fracture of the local crust.

Acknowledgments. I would like to thank Takashi Yanagidani for discussion and suggestion. I would also like to thank Shoji Ehara for discussion and assistance in the experiment. I greatly appreciate the advice and comments of Keisuke Ito and Osam Sano, who read the manuscript.

REFERENCES

Akaike, H., A new look at the statistical model identification, *IEEE Trans. Control, AC-19*, 716–723, 1974.

Allégre, C. J., J. L. Le Mouel, and A. Provost, Scaling rules in rock fracture and possible implications for earthquake prediction, *Nature, 297*, 47–49, 1982.

Brown, S. R., and C. H Scholz, Broad bandwidth study of the topography of natural rock surfaces, *J. Geophys. Res., 90*, 12,575–12,582, 1985.

Davidon, W. C., Variance algorithm for minimization, *Comput. J. 10*, 406–410, 1968.

Hirata, T., T. Yanagidani, and M. Terada, Time series measurement system of AE events, in *Progress in Acoustic Emission II: Proceedings of the 7th International Acoustic Emission Symposium,*

edited by M. Onoe, K. Yamaguchi, and H. Takahashi, pp. 359–365, Japanese Society for Non-Destructive Inspection, Tokyo, 1984.

Hirata, T., T. Satoh, and K. Ito, Fractal structure of spatial distribution of microfracturing in rock, *Geophys. J. R. Astron. Soc.*, in press, 1987.

Kagan, Y. Y., and L. Knopoff, Statistical study of the occurrence of shallow earthquakes, *Geophys. J. R. Astron. Soc.*, *55*, 67–86, 1978.

Kagan, Y., and L. Knopoff, Spatial distribution of earthquakes: The two-point correlation function, *Geophys. J. R. Astron. Soc.*, *62*, 303–320, 1980*a*.

Kagan, Y. Y., and L. Knopoff, Dependence of seismicity on depth, *Bull. Seimsol. Soc. Am.*, *70*, 1811–1822, 1980*b*.

Kagan, Y. Y., and L. Knopoff, Stochastic synthesis of earthquake catalogs, *J. Geophys. Res.*, *86*, 2853–2862, 1981.

King, G., The accommodation of large strains in the upper lithosphere of the earth and other solids by self-similar fault systems: The geometrical origin of *b*-value, *Pure Appl. Geophys.*, *121*, 761–815, 1983.

Liptser, R. S., and A. N. Shiryayev, *Statistics of Random Processes, II, Applications*, 339 pp., Springer-Verlag, New York, 1978.

Madden, T. R., Microcrack connectivity in rocks: a renormalization group approach to the critical phenomena of conduction and failure in crystalline rocks, *J. Geophys. Res.*, *88*, 585–592, 1983.

Mandelbrot, B. B., How long is the coast of Britain?, *Science*, *155*, 636–638, 1967.

Mikumo, T, and T. Miyatake, Earthquake sequences on a frictional fault model with non-uniform strengths and relaxation times, *Geophys. J. R. Astron. Soc.*, *59*, 497–522, 1979.

Mogi, K., Study of elastic shocks caused by the fracture of heterogeneous materials and its relations to earthquake phenomena, *Bull. Earthquake Res. Inst. Tokyo Univ.*, *40*, 125–173, 1962.

Ogata, Y., Estimation of the parameters in the modified Omori's formula for aftershock frequencies by the maximum likelihood procedure, *J. Phys. Earth*, *31*, 115–124, 1983.

Sadovskiy, M. A., T. V. Golubeva, V. F. Pisarenko, and M. G. Shnirman, Characteristic dimensions of rock and hierarchical properties of seismicity, *Izv. Acad. Sci. USSR Earth Phys*, Engl. Transl., *20*, 87–96, 1984.

Scholz, C. H., Microfractures, aftershocks, and seismicity, *Bull. Seismol. Soc. Am*, *58*, 1117–1130, 1968*a*.

Scholz, C. H., The frequency-magnitude relation of microfracturing in rock and its relation to earthquakes, *Bull. Seismol. Soc. Am.*, *58*, 399–415, 1968*b*.

Scholz, C. H., and C. A. Aviles, The fractal geometry of faults and faulting, in *Earthquake Source Mechanics, Geophys. Monogr. Ser.*, vol. 37, edited by S. Das, J. Boatwright, and C. H. Scholz, pp. 147–155, AGU, Washington, D. C., 1986.

Smalley, R. F., D. L. Turcotte, and S. A. Solla, A renormalization group approach to the stick-slip behavior of faults, *J. Geophys. Res.*, *90*, 1894–1900, 1985.

Turcotte, D. L., Fractals and fragmentation, *J. Geophys. Res.*, *91*, 1921–1926, 1986.

Turcotte, D. L., R. F. Smalley, and S. A. Solla, Collapse of loaded fractal trees, *Nature*, *313*, 671–672, 1985.

T. Hirata, Department of Geophysics, Faculty of Science, Kyoto University, Kyoto 606, Japan.

(Received October 10, 1986;
revised February 3, 1987;
accepted February 12, 1987.)